# Supporting Information

# Harnessing mpg-$C_3N_4$ Photocatalyst for Selective Oxidative Coupling of Amines to Azoaromatics Compounds

Dinesh S. Chaudhari,[a] Rahul P. Gaikwad,[a] Indrajeet R. Warkad,[a] Rostislav Langer,[b] Michal Otyepka,[b,c] and Manoj B. Gawande[a,d]*

[a]Department of Industrial and Engineering Chemistry, Institute of Chemical Technology, Mumbai, Marathwada Campus, Jalna-431213 Maharashtra, India.
[b]IT4Innovations, VSB – Technical University of Ostrava, 17. listopadu 2172/15, 708 00 Ostrava-Poruba, Czech Republic.
[c]Regional Centre of Advanced Technologies and Materials, The Czech Advanced Technology and Research Institute (CATRIN), Palacký University Olomouc, Šlechtitelů 27, 779 00 Olomouc, Czech Republic.
[d]Nanotechnology Centre, Centre for Energy and Environmental Technologies, VŠB–Technical University of Ostrava, 17. Listopadu 2172/15, 708 00 Ostrava-Poruba, Czech Republic.

*Corresponding author: Prof. Manoj B. Gawande (mb.gawande@marj.ictmumbai.edu.in)

Postal address: Department of Industrial and Engineering Chemistry, Institute of Chemical Technology, Mumbai, Marathwada Campus, Jalna-431213 Maharashtra, India

## 1. Experimental section

### 1.1 Materials

Urea, melamine, dimethyl sulfoxide (DMSO), and other necessary reagents, along with various amine substrates, were obtained from commercial suppliers, including Sigma-Aldrich, Avra, BLD Pharma, and Molychem, India. These materials were utilized in their original form without further purification, unless otherwise specified. All the solvents used were of analytical grade. The 395 nm (36 W) light source was purchased from the RDR Store (https://www.rdrstore.in).

### 1.2 Synthesis of mpg-$C_3N_4$

The synthesis of mpg-$C_3N_4$ was conducted through a one-step thermal polymerization method, as outlined in our previous research,[1] with some modifications. Specifically, 15 g of urea was

placed in a porcelain crucible and then set inside a muffle furnace. The material was heated to 550 °C, increasing the temperature by 50 °C every 10 minutes, and held at this temperature for 2 hours, resulting in a light-yellow material after cooling to room temperature known as mpg-$C_3N_4$.

### 1.3 Synthesis of Bulk-$C_3N_4$

Bulk-$C_3N_4$ was synthesized using a similar method, substituting urea with melamine. In this procedure, 15 g of melamine was placed in a porcelain crucible and then set inside a muffle furnace. The material was gradually heated to 550 °C, with the temperature rising by 50 °C every 10 minutes, and then kept at this temperature for 2 hours, resulting in the production of bulk-$C_3N_4$.

### 1.3 Catalysts characterization

The characterization of the synthesized materials was conducted using a range of advanced techniques. Powder X-ray diffraction (PXRD) patterns were obtained using a Bruker D8 Advance X-ray diffractometer with Cu-Kα radiation (λ = 1.5418 Å). Infrared spectroscopy was performed with an FT/IR 6600 JASCO instrument covering a spectral range from 500 $cm^{-1}$ to 4000 $cm^{-1}$. The surface morphology of the catalyst was examined using transmission electron microscopy (TEM), with high-resolution TEM (HRTEM) imaging and energy-dispersive X-ray (EDX) mapping conducted on a JEOL JEM 2100 PLUS model. X-ray photoelectron spectroscopy (XPS), employing an Al Kα radiation source and ultra-high vacuum monochromator, was used to determine the elemental composition of the samples. The BET surface area and pore size distribution were measured through N2 adsorption/desorption isotherms at 77 K using a BELSORP MAX II instrument. A Shimadzu UV-visible spectrophotometer was utilized to measure the diffuse reflectance spectra of the carbon nitride sample, with barium sulfate serving as the reference. FP-8200/Jasco instrument was employed to record the Solid-state Photoluminescence spectra (PL). Temperature-programmed desorption (TPD) measurements were performed on BELCAT II system configured with a thermal conductivity detector (TCD). Prior to $CO_2$-TPD analysis, the sample was degassed for 1.5 hours at 200 °C in a helium atmosphere and then cooled to 50 °C. Following cooling, the sample was purged with $CO_2$ gas (99.99%) for 30 minutes. Any physically adsorbed $CO_2$ was subsequently removed with helium gas before heating the sample to 600 °C at a ramp rate of 10 °C/min followed by a 20-minute hold. $CO_2$ desorption was measured using the TCD

detector. Electron paramagnetic resonance (EPR) spectroscopy was performed at room temperature with a JEOL JES-FA200 ESR Spectrometer operating in both X and Q bands.

### 1.4 Photo-electrochemical measurement

Photo-electrochemical investigations were conducted using a Metrohm Autolab workstation set up in a three-electrode configuration, comprising a platinum wire as the counter electrode, a KCl-saturated Ag/AgCl electrode as the reference, and a carbon nitride-coated fluorine-doped tin oxide (FTO) electrode (1 cm x 1 cm) as the working electrode. A 0.2 M aqueous solution of $Na_2SO_4$ was used as the electrolyte. The working electrode was prepared by coating a slurry of carbon nitride (mpg-$C_3N_4$ or bulk-$C_3N_4$) onto the FTO electrode, thereafter dried overnight at ambient temperature. The carbon nitride slurry was made by suspending 2 mg of catalyst in 0.2 mL of isopropanol, along with 20 µL of a 10% Nafion solution in ethanol, using ultrasonication for 1 hour. A 300 W Xenon lamp (ASAHI Spectra) emitting visible light in the range of 400-700 nm was utilized as the illumination source for the photocurrent study. Electrochemical impedance spectroscopy (EIS) was also carried out, and Nyquist plots were obtained over a frequency range of 0.01 Hz to 106 Hz in the 0.2 M $Na_2SO_4$ solution at open circuit potential. Linear Sweep Voltammetry (LSV) measurements were conducted over a potential window of 0 to +1.5 V at a scan rate of 0.02 mV/s.

### 1.5 Computational details

All calculations were carried out according to the density functional theory (DFT) with Gaussian software.[2] Geometry optimizations for all species studied were performed using the unrestricted $\omega$B97X-D functional[3] in combination with the Karlsruhe def2-TZVP basis set.[4] The influence of the solvent were simulated employing the universal continuum solvation model relies on electron density (SMD)[5] and the relative permittivity 46.8 representing the DMSO solvent. The temperature was set to 313 K in agreement with the experimental conditions. All Gibbs free energies were determined at 313 K and 1 atm employing standard statistical thermodynamics, incorporating the rigid rotor, harmonic oscillator, and ideal gas models. Due to the high computational cost of frequency calculations at the triple-zeta level with respect to the used models, reaction Gibbs energies were estimated as: $\Delta G = E_{SCF}^{def2-TZVP} + G_{thermal}^{def2-SVP}$, where $E_{SCF}^{def2-TZVP}$ denotes electronic energies optimized on

def2-TZVP level, and $G_{thermal}^{def2-SVP}$ represents thermal corrections to Gibbs free energies derived from frequency calculations using def2-SVP basis set.

Adsorption Gibbs energies, $\Delta G_{ads}$, were evaluated as: $\Delta G_{ads} = G_{cat+mol} - G_{cat} - G_{mol}$, where $G_{cat+mol}$, $G_{cat}$, and $G_{mol}$ represent the Gibbs energies of mpg-$C_3N_4$ catalyst with adsorbed molecule, pristine mpg-$C_3N_4$ catalyst, and isolated molecule, respectively. Wiberg bond indices (WBIs) were calculated to elucidate the bond order characteristics of adsorbed $O_2$ species.[6, 7]

**1.6 General procedure for photocatalytic oxidative coupling of arylamines**

The photocatalytic oxidative coupling reaction was carried out in a round-bottom flask (RB) under ambient conditions. In a typical setup, 0.1 mmol of the amine substrate, 30 mg of the mpg-$C_3N_4$ photocatalyst, 3 mL of DMSO, and 1 equivalent of dodecane (used as an internal standard) were introduced into a 10 mL round-bottom flask with a subsequent introduction of 1 equivalent of $K_3PO_4$. The reaction mass was stirred continuously for 24 hours while being exposed to light from a 395 nm lamp (36 W) under open-air conditions. Upon completion of the reaction, the mixture and photocatalyst were separated via centrifugation. The resulting solution was then diluted with methanol and examined using gas chromatography-mass spectrometry (GC-MS).

For the recycling study, the photocatalyst was recovered through centrifugation and washed several times with DMSO, water, and ethanol, followed by drying in a laboratory oven at 70 °C for 12 hours before being reused in the subsequent reaction cycle.

**1.7 Method of reaction product analysis**

The reaction progress was tracked at various time points and quantified using a SHIMADZU GC-MS-QP2020 system, fitted with an SH-Rxi-5Sil MS column (30 m x 0.25 mm x 0.25 μm) and QP2020 mass detector.

The conversion of amines and the selectivity of the products were calculated using the formulas outlined below.

Conversion (%) = $\{Co - Ct/Co\} \times 100$

where *Co* is the reactant's initial concentration, and *Ct* is the concentration of the reactant at time t.

Selectivity (%) = $\{Cp/Co - Ct\} \times 100$

where *Cp* is the concentration of the product at time t, *Co* is the reactant's initial concentration, and

*Ct* is the reactant concentration at time t.

### 1.8 Radical trapping experiment

Radical trapping experiments were carried out using 2,6-di-tert-butyl-4-methylphenol (BHT) to capture the amine radical. Briefly, 0.1 mmol of *p*-anisidine, $K_3PO_4$ (1eq.), mpg-$C_3N_4$ (30 mg), and BHT (2 eq.) in 3 mL of DMSO were stirred under an air atmosphere with light irradiation from a 395 nm lamp for 24 hours. After 24 hours of irradiation, the reaction mass was analyzed using HR-MS and GC-MS.

### 1.9 Electron paramagnetic resonance experiment

Electron paramagnetic resonance (EPR) study was conducted to verify the existence of superoxide radicals in the reaction mixture. The spin-trapping agent used was 5,5-dimethyl-1-pyrroline-N-oxide (DMPO), and the EPR signals were obtained using a JEOL EPR spectrometer (JES-FA200). In a standard procedure, a mixture containing 0.1 mmol of compound **1a**, 50 mM DMPO, 1 equivalent of $K_3PO_4$, and 30 mg of mpg-$C_3N_4$ in DMSO (3 mL) was stirred at ambient temperature under an air atmosphere. EPR signals were recorded both in the dark and after 5 minutes of exposure to light from a 395 nm lamp.

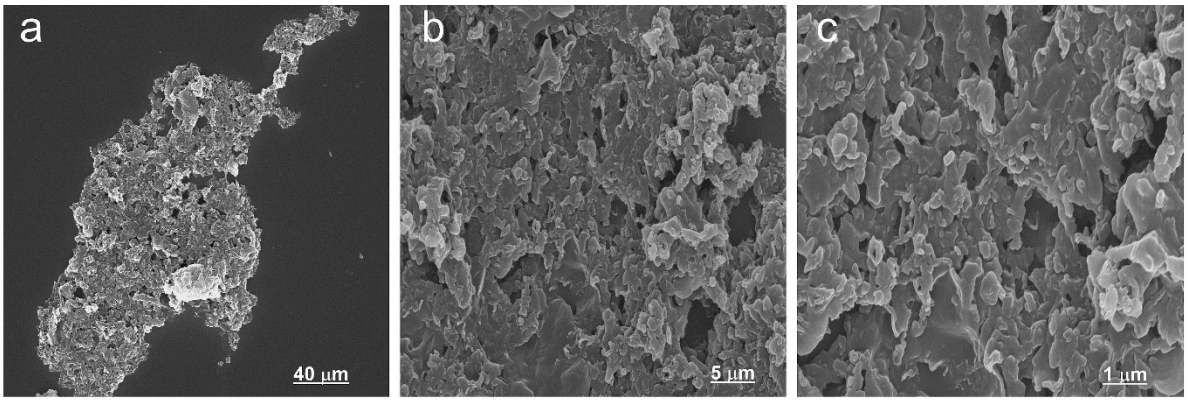


**Figure S1**. SEM images of mpg-$C_3N_4$.

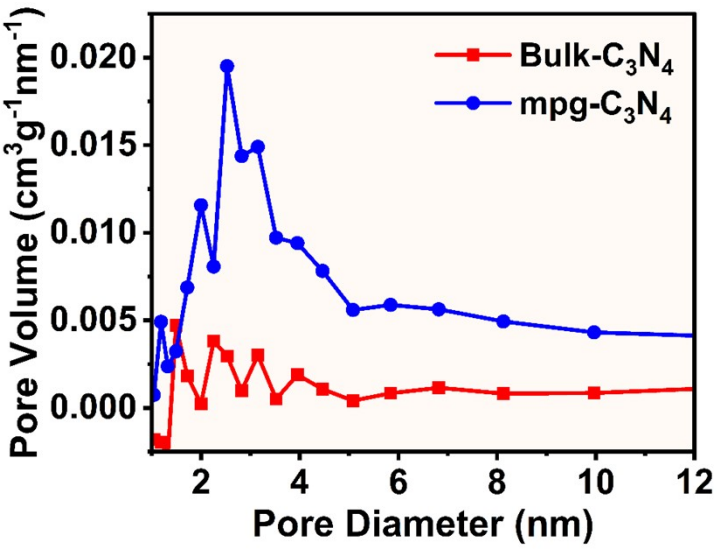


**Figure S2**. Pore size distribution of mpg-$C_3N_4$ and bulk-$C_3N_4$ (BJH plot).

**Table S1**. Porosity characteristics of mpg-$C_3N_4$ and bulk-$C_3N_4$

| Sample | $S_{BET}$ ($m^2$ $g^{-1}$) | Total pore volume[a] (p/p0=0.99) [$cm^3$ $g^{-1}$] | Average pore diameter[b] (nm) |
|---|---|---|---|
| Bulk-$C_3N_4$ | 20.64 | 0.1554 | 31.205 |
| mpg-$C_3N_4$ | 109.40 | 0.8025 | 28.17 |

[a] Total pore volume derived from the adsorbed quantity at a relative pressure of *p/p0*=0.99.

[b] Average pore diameters estimated from the adsorption branches of the isotherms by employing the BJH method.

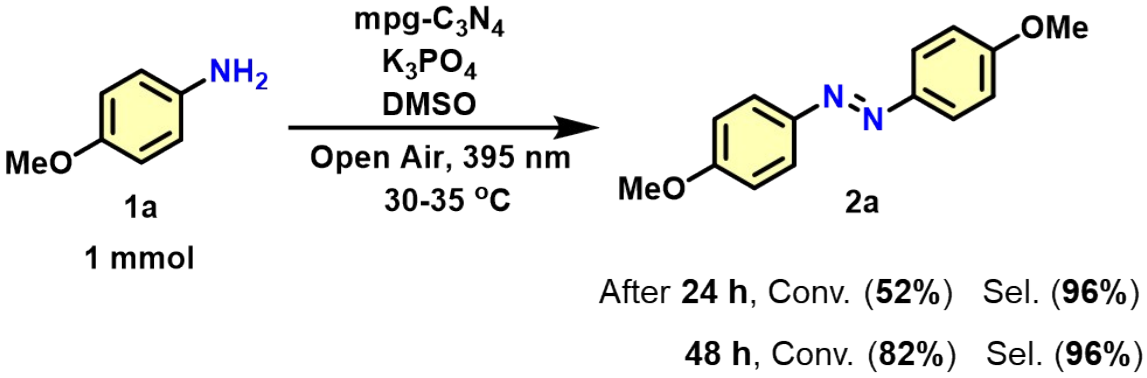


**Figure S3**. Scale-up study. Reaction condition: *p*-anisidine (**1a**) (1 mmol), mpg-$C_3N_4$ (300 mg), $K_3PO_4$ (1 eq.), DMSO (30 mL), air atmosphere, 395 nm lamp (36 W), 30-35 °C. Conversion and selectivity were measured by GC-MS analysis utilizing dodecane as the internal standard.

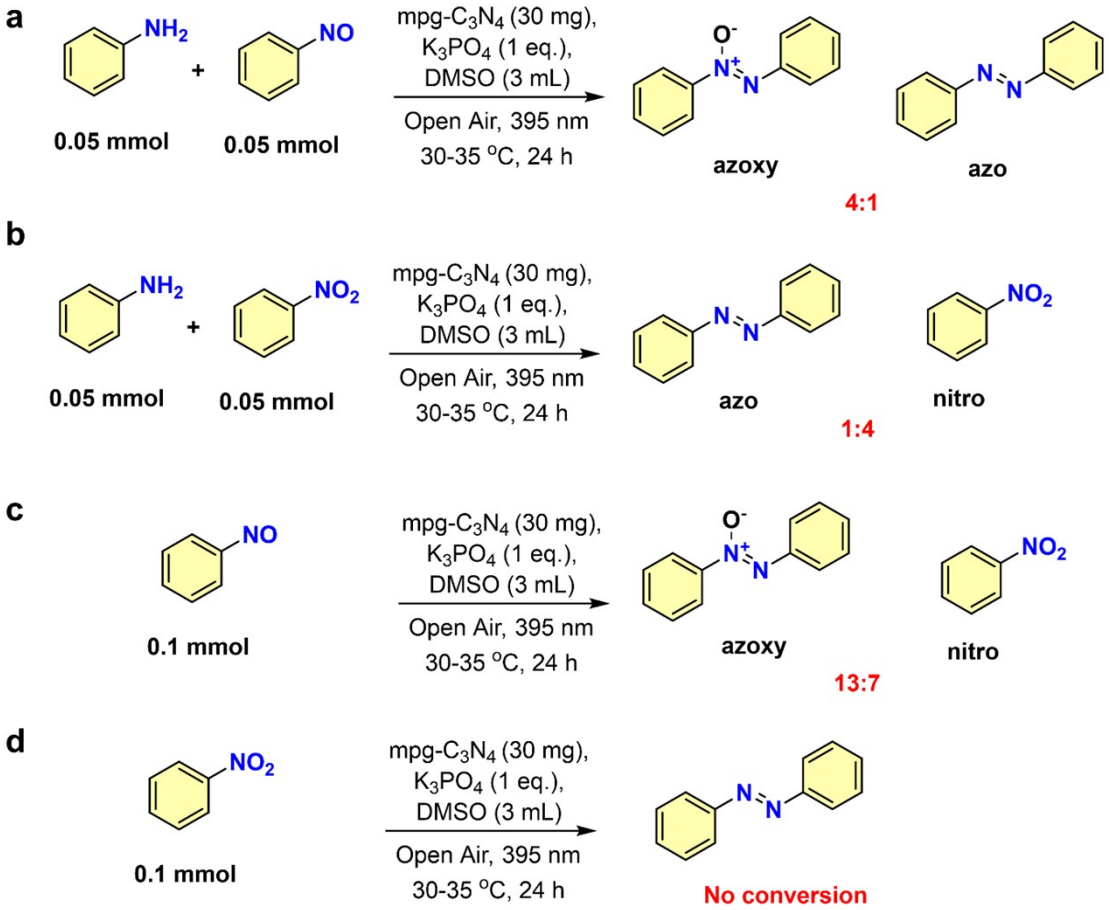


**Figure S4**. Control experiments for the mechanistic investigation of photocatalytic oxidative coupling of arylamines.

To assess the involvement of the oxygen-containing species (such as nitroso or nitro compounds) in the reaction pathway, we conducted a control test using equal mixtures of aniline with either nitrosobenzene or nitrobenzene under optimal conditions (**Fig. S4a-b**). After 24 hours of light irradiation, GC-MS analysis of the reaction mixtures showed that the combination of aniline and nitrosobenzene produced a 4:1 ratio of azoxybenzene to azobenzene, while the reaction with nitrobenzene yielded a 1:4 ratio of azobenzene to nitrobenzene. In contrast, reactions using only nitrosobenzene or nitrobenzene did not result in the formation of azobenzene (**Fig. S4c-d**). These product distributions differ significantly from those observed when aniline was the sole substrate under standard conditions (**Table 2**, entry **2n**). Therefore, these results suggest that oxygenated intermediates are unlikely to be involved in the reaction mechanism.

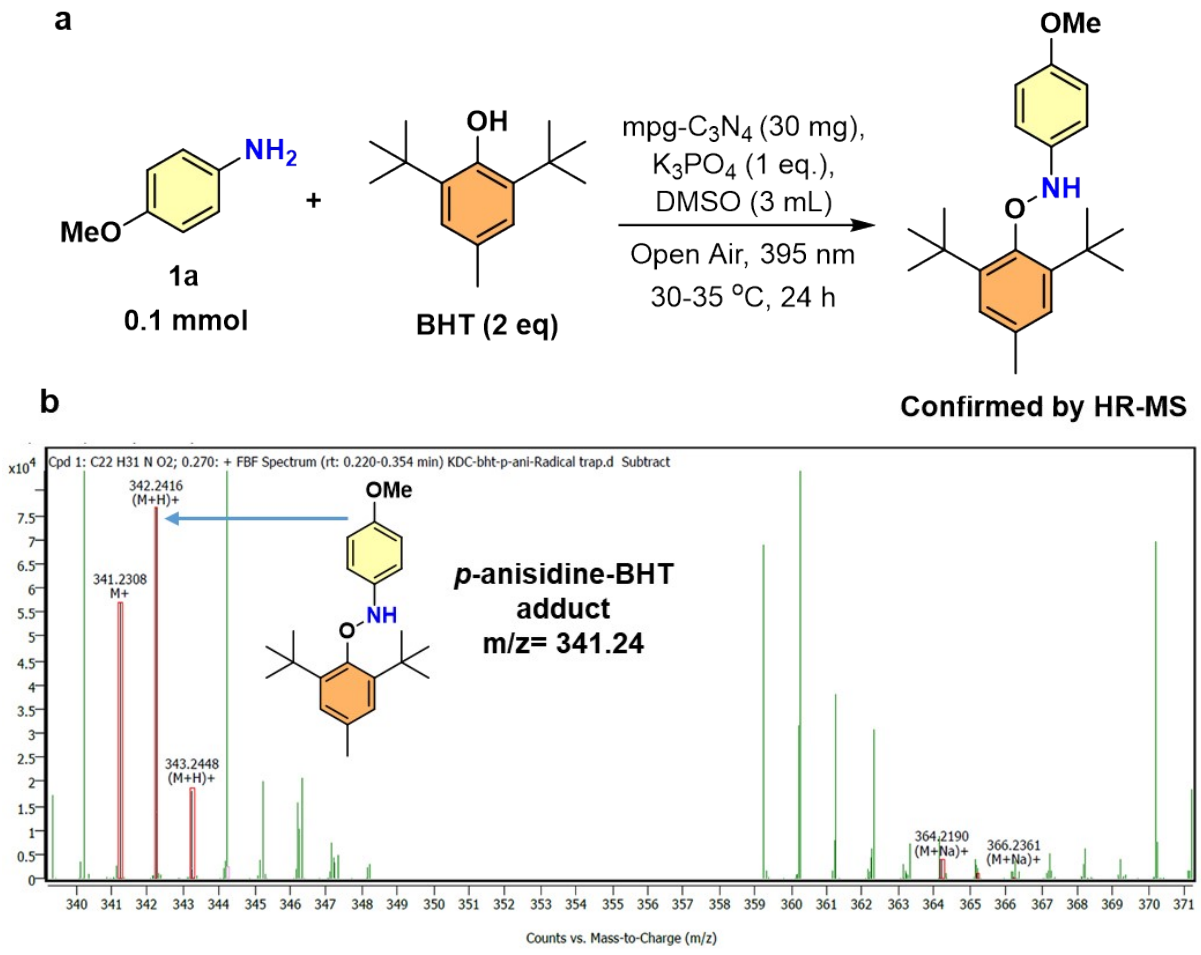


**Figure S5**. (a) Radical trap experiment with BHT, (b) Obtained HR-MS spectra of the *p*-anisidine-BHT adduct after the radical trap experiment.

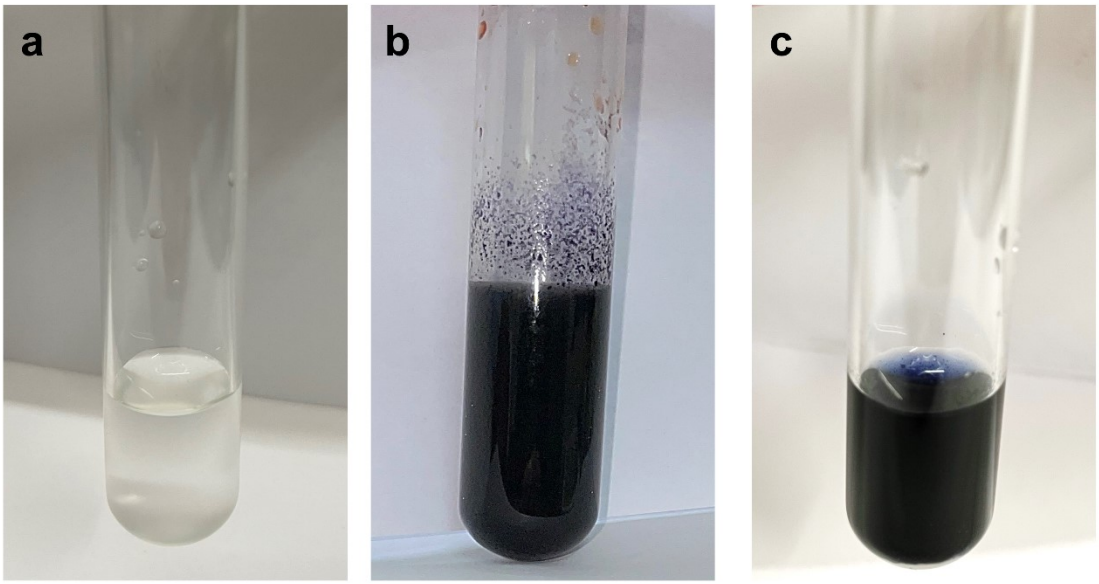


**Figure S6**. Detection of the $H_2O_2$ in the reaction mixture of photocatalytic oxidative coupling of arylamines. (a) The optical image of KI, aqueous acetic acid, and starch. (b) The optical image of KI, aqueous acetic acid, starch, and the *p*-toluidine oxidation reaction mixture (Under standard reaction conditions). (c) The optical image of KI, aqueous acetic acid, starch, and the 30% $H_2O_2$ (Standard).

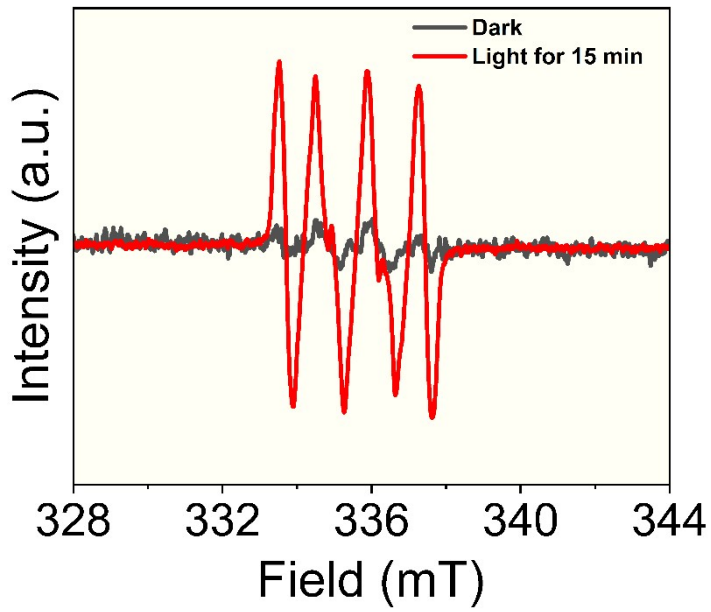


**Figure S7**. EPR spectrum of superoxide radicals formed by the mpg-$C_3N_4$ photocatalyst under dark and light irradiation.

| Catalyst | Type | Conditions | Source of light/ Temp. | Yield (%) | Ref. |
|---|---|---|---|---|---|
| $[W(O)_2(Cl)^{4\text{-}MeO}bpy]_2O$ | Homogeneous | $H_2O_2$+$O_2$, AcOH, 12h | 55 °C | 94 | [8] |
| h-CoNC | Heterogeneous | $O_2$, KOH, DMSO, 24h | R.T. | 74 | [9] |
| $Zr(OH)_4$ | Heterogeneous | TBHP, AcOH, 24h | 40 °C | 74 | [10] |
| $Th_6$-C8A | Heterogeneous | $H_2O_2$, AcOH, 48h | R.T. | 26 | [11] |
| Molybdenum-based catalyst | Homogeneous | $H_2O_2$, $Na_2S_2O_3$ MeOH, 24h | 60 °C | 69 | [12] |
| $Ir(dF\text{-}CF_3\text{-}ppy)_2(dtbpy)^+ PF_6^-$ | Homogeneous | Air, $K_3PO_4$, $CH_3CN$, 24h | λ= 450 nm | 67 | [13] |
| MnOOH nanotubes | Heterogeneous | $O_2$ (5 bar) Toluene, 24h | 60 °C | 99 | [14] |
| $RuO_2/Cu_2O$ NPs | Heterogeneous | Air, $CH_3CN$, 16h | 85 °C | 98 | [15] |
| DPZ-TPY | Homogeneous | Air, KOH, DMSO-$H_2O$, 24h | Visible light | 86 | [16] |
| Bimetallic $Ag_{0.75}Ni_{0.25}$ alloy | Heterogeneous | $H_2O_2$, KOH $CH_3CN$, 6h | Visible light | 95 | [17] |
| meso-$Mn_2O_3$ | Heterogeneous | Air, Toluene, 12h | 110 °C | 89 | [18] |
| Ag nanoparticles | Heterogeneous | Air, KOH, DMSO, 24h | R.T. | 91 | [19] |
| CuBr | Homogeneous | $O_2$, Pyridine, Toluene, 20h | 60 °C | 66 | [20] |
| $Au/TiO_2$ | Heterogeneous | $O_2$ (5 bar) Toluene, 5h | 100 °C | 89 | [21] |
| **mpg-$C_3N_4$ (Metal-free)** | **Heterogeneous** | Air, $K_3PO_4$, DMSO, 24h | λ= 395 nm | **97** | **This work** |

**Table S2**. Recent reports on the synthesis of azo compounds

**GC-MS Data:**

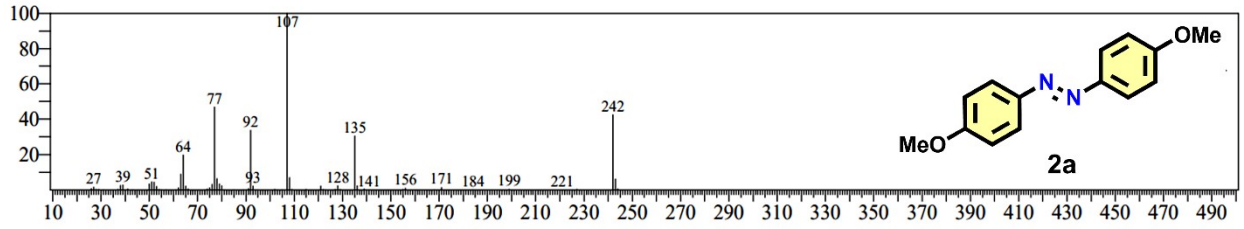
OMe
MeO
2a

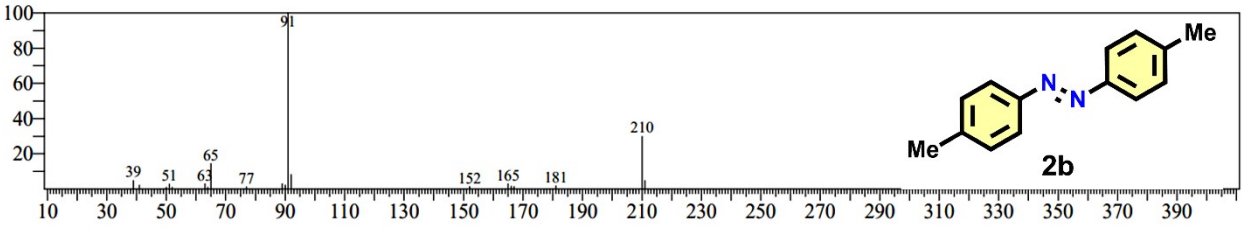
Me
Me
2b

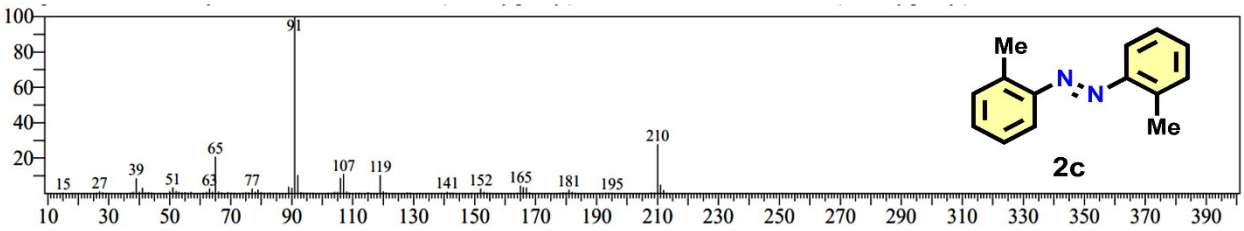
Me
Me
2c

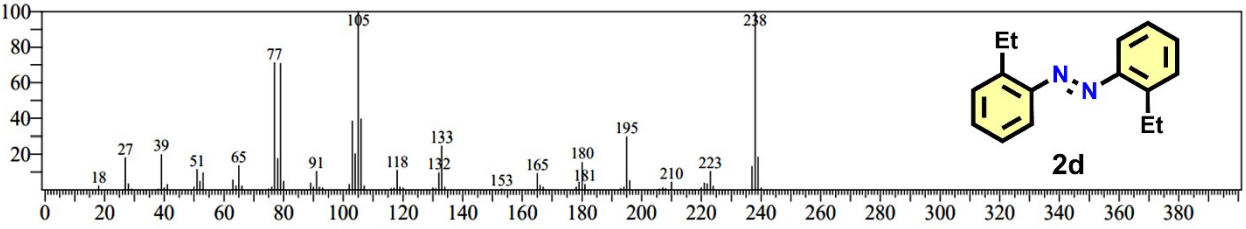
Et
Et
2d

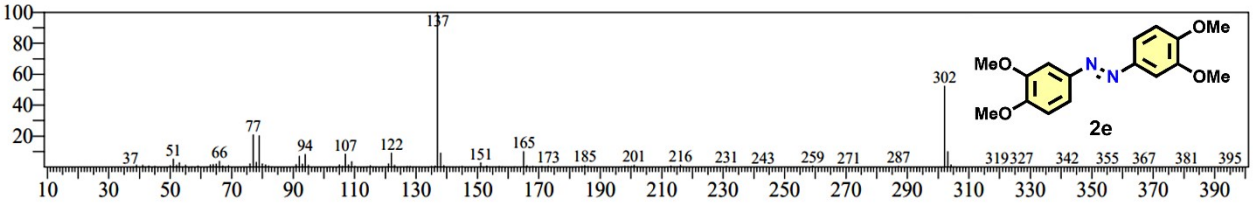
OMe
MeO
MeO
OMe
2e

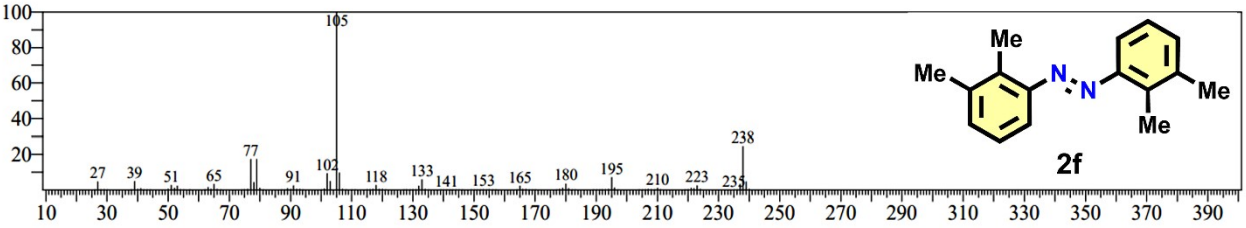
Me
Me
Me
Me
2f

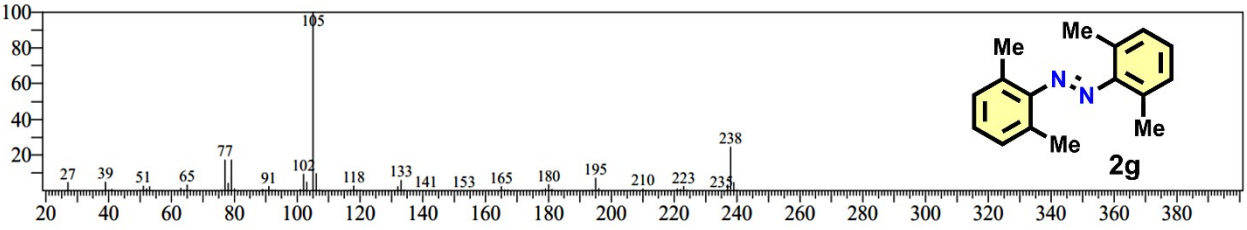
Me
Me
Me
Me
2g

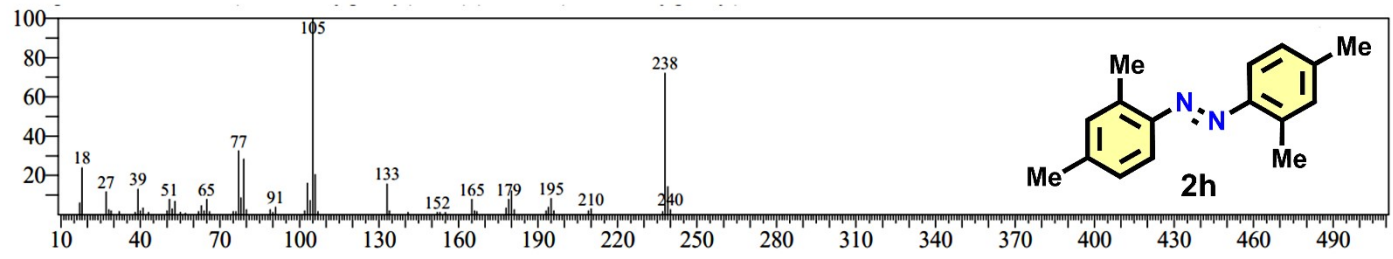
105
238
77
18
27
39
51
65
91
133
152
165
179
195
210
240
Me
Me
Me
Me
N
N
2h

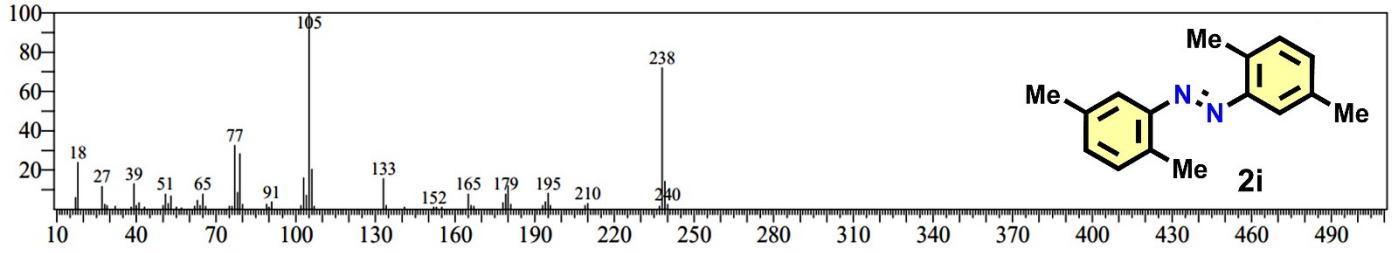
105
238
77
18
27
39
51
65
91
133
152
165
179
195
210
240
Me
Me
Me
Me
N
N
2i

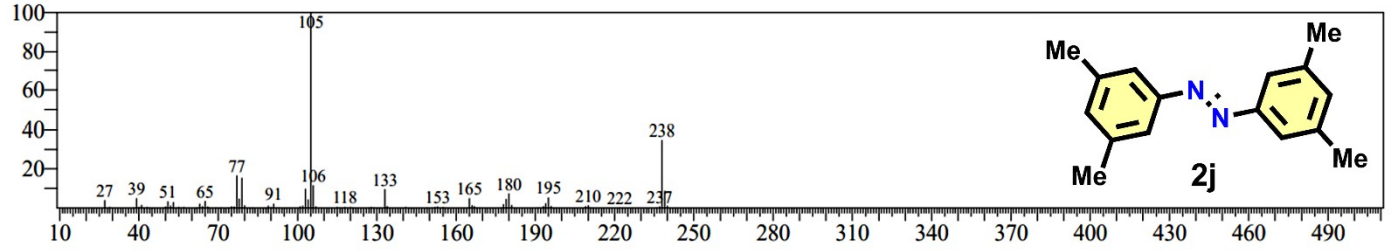
105
238
77
106
27
39
51
65
91
118
133
153
165
180
195
210
222
237
Me
Me
Me
Me
N
N
2j

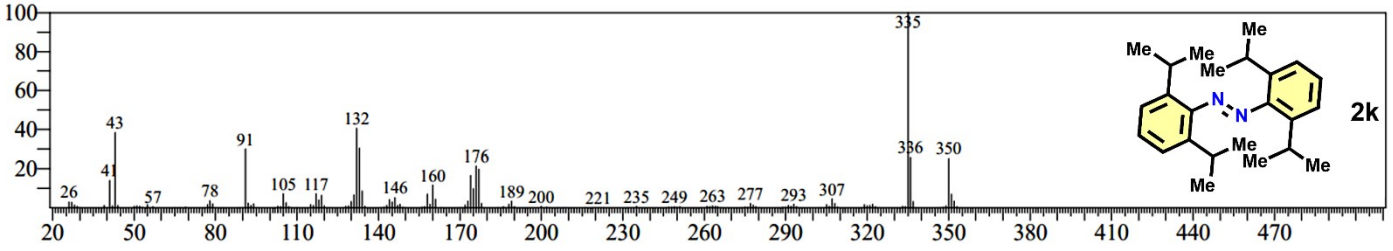
335
43
41
91
132
176
26
57
78
105
117
146
160
189
200
221
235
249
263
277
293
307
336
350
Me
Me
Me
Me
Me
Me
Me
Me
N
N
2k

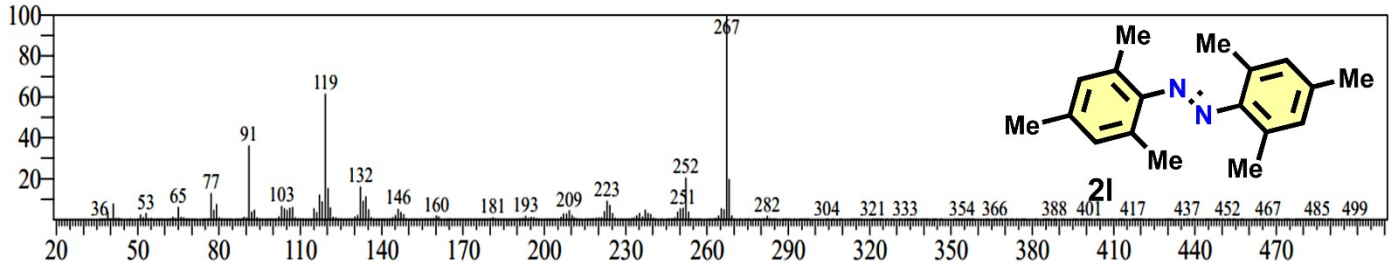
267
119
91
77
132
103
146
160
181
193
209
223
252
251
36
53
65
282
304
321
333
354
366
388
401
417
437
452
467
485
499
Me
Me
Me
Me
Me
Me
N
N
2l

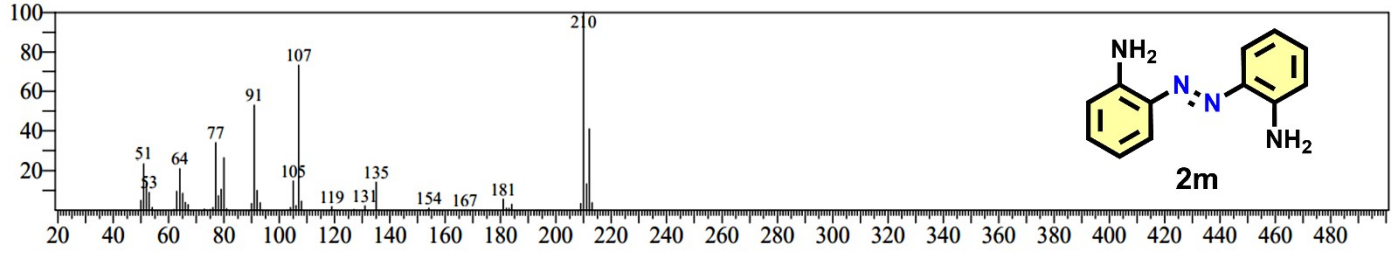
210
107
91
77
51
64
53
105
135
119
131
154
167
181
NH2
NH2
N
N
2m

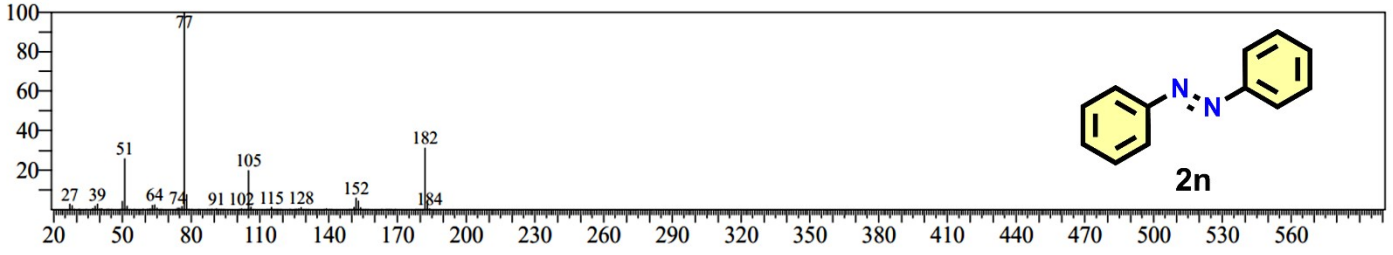
77
51
105
182
27
39
64
74
91
102
115
128
152
184
N
N
2n

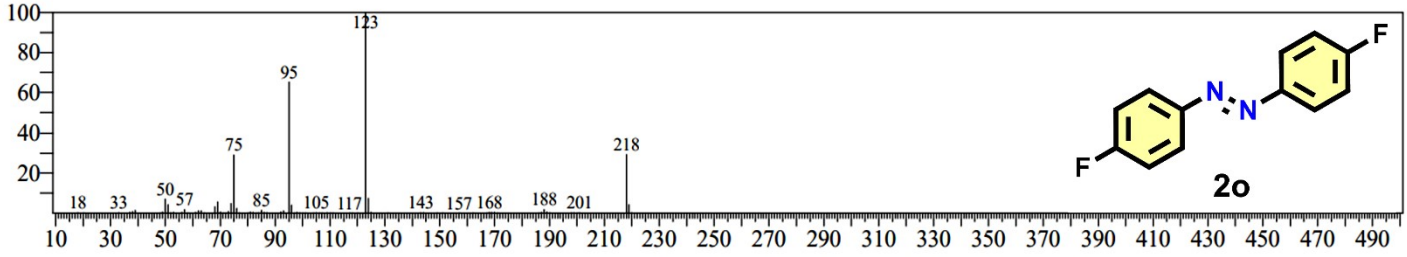
123
95
75
218
F
F
N
N
2o

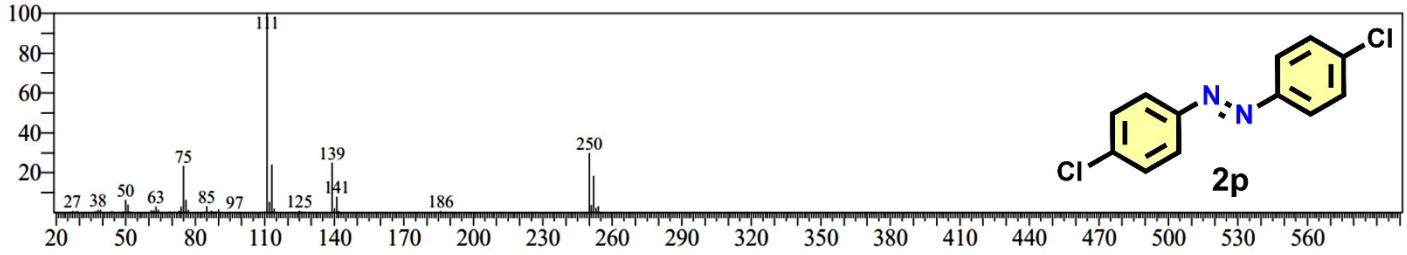
111
75
139
141
250
Cl
Cl
N
N
2p

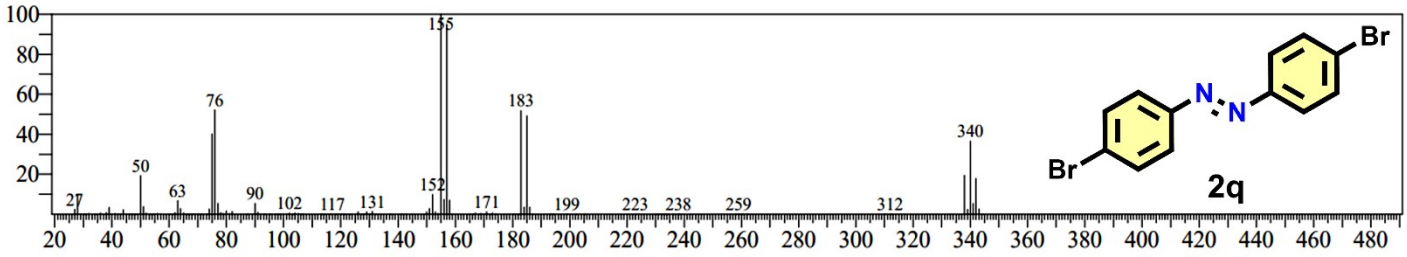
155
76
183
340
50
152
Br
Br
N
N
2q

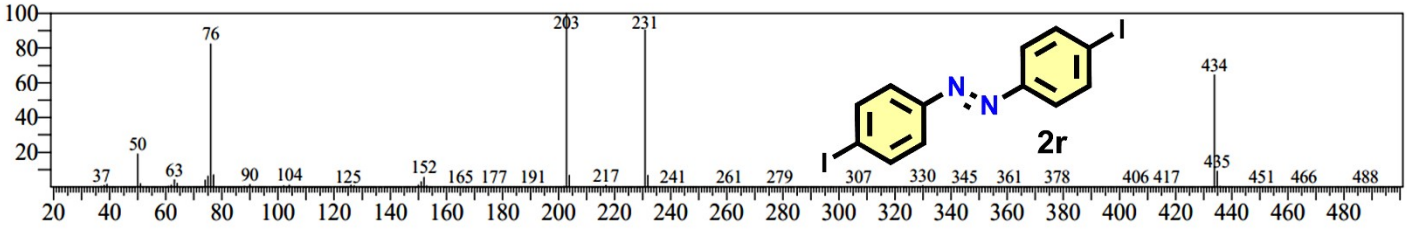
203
231
76
434
50
435
I
I
N
N
2r

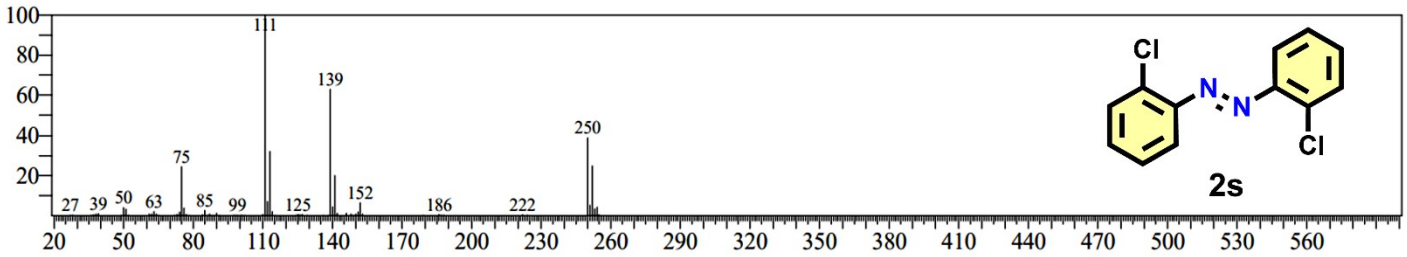
111
139
250
75
152
Cl
Cl
N
N
2s

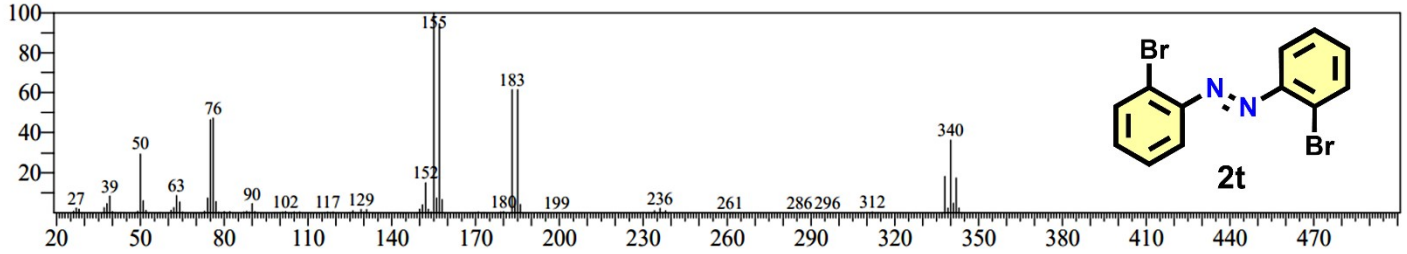
155
183
76
340
50
152
Br
Br
N
N
2t

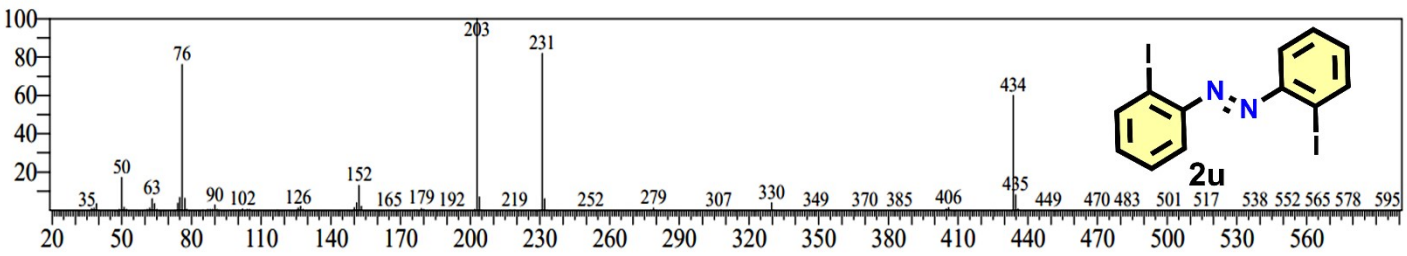
203
231
76
434
50
152
435
I
I
N
N
2u

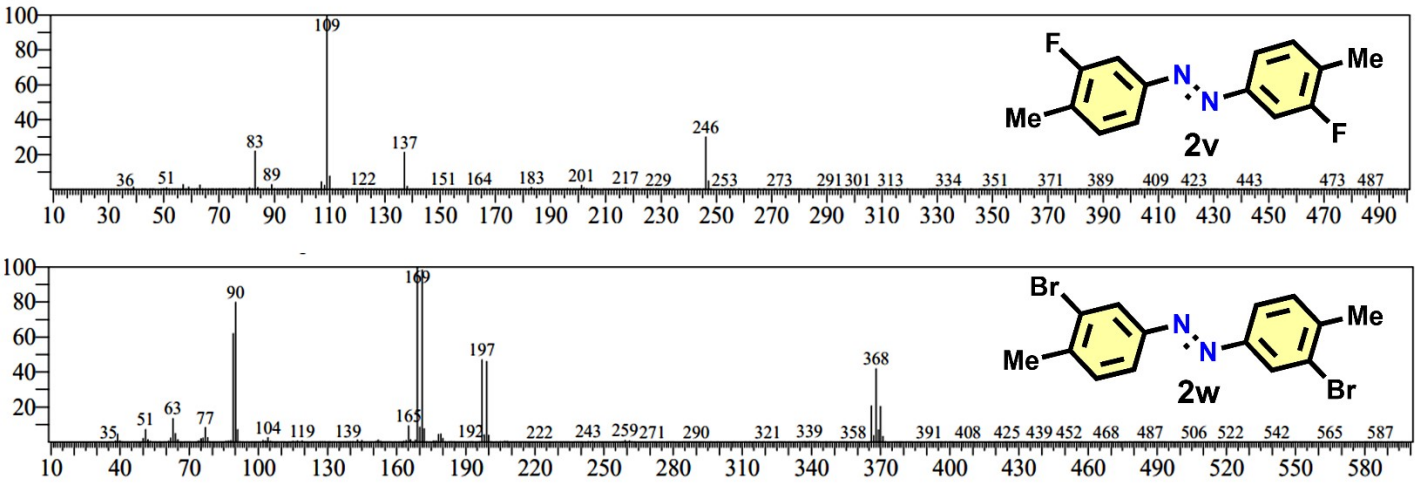


## References


[1] R. P. Gaikwad, D. R. Naikwadi, A. V. Biradar, M. B. Gawande, *ACS Appl. Nano Mater.* 2023, **6**, 1859-1869.

[2] M. J. Frisch, G. W. Trucks, H. B. Schlegel, G. E. Scuseria, M. A. Robb, J. R. Cheeseman, G. Scalmani, V. Barone, G. A. Petersson, H. Nakatsuji, X. Li, M. Caricato, A. V. Marenich, J. Bloino, B. G. Janesko, R. Gomperts, B. Mennucci, H. P. Hratchian, J. V. Ortiz, A. F. Izmaylov, J. L. Sonnenberg, D. Williams-Young, F. Ding, F. Lipparini, F. Egidi, J. Goings, B. Peng, A. Petrone, T. Henderson, D. Ranasinghe, V. G. Zakrzewski, J. Gao, N. Rega, G. Zheng, W. Liang, M. Hada, M. Ehara, K. Toyota, R. Fukuda, J. Hasegawa, M. Ishida, T. Nakajima, Y. Honda, O. Kitao, H. Nakai, T. Vreven, K. Throssell, J. A. Montgomery, Jr., J. E. Peralta, F. Ogliaro, M. J. Bearpark, J. J. Heyd, E. N. Brothers, K. N. Kudin, V. N. Staroverov, T. A. Keith, R. Kobayashi, J. Normand, K. Raghavachari, A. P. Rendell, J. C. Burant, S. S. Iyengar, J. Tomasi, M. Cossi, J. M. Millam, M. Klene, C. Adamo, R. Cammi, J. W. Ochterski, R. L. Martin, K. Morokuma, O. Farkas, J. B. Foresman, and D. J. Fox, *Gaussian, Inc., Wallingford CT*, 2016.

[3] J.-D. Chai, M. Head-Gordon, *Phys. Chem. Chem. Phys*. 2008, **10**, 6615–6620.

[4] F. Weigend, R. Ahlrichs, *Phys. Chem. Chem. Phys.* 2005, **7**, 3297–3305.

[5] A. V. Marenich, C. J. Cramer, D. G. Truhlar, *J. Phys. Chem. B* 2009, **113**, 6378–6396.

[6] A. Reed, F. Weinhold, *J. Chem. Phys.* 1983, **78**, 4066–4073.

[7] K. B. Wiberg, *Tetrahedron* 1968, **24**, 1083–1096.

[8] H. Song, J. Wei, Z. Wang, Y. Liu, S. Zhao, X. Cai, Y. Xiao, L. Yang, P. Bai, L. Fang, F. Yang, S. Zheng, W. Zhang, J. Pan, C. Xu, *ACS Catal.* 2024, **14**, 12372-12384.

[9] X. Han, T. Zhang, X. Wang, Z. Zhang, Y. Li, Y. Qin, B. Wang, A. Han, J. Liu, *Nat. Commun.* 2022, **13**, 2900.

[10] J. Qin, Y. Long, F. Sun, P.-P. Zhou, W. D. Wang, N. Luo, J. Ma, *Angew. Chem. Int. Ed.* 2022, **61**, e202112907.

[11] Q. Niu, Q. Huang, T.-Y. Yu, J. Liu, J.-W. Shi, L.-Z. Dong, S.-L. Li, Y.-Q. Lan, *J. Am. Chem. Soc.* 2022, **144**, 18586-18594.

[12] S. Han, Y. Cheng, S. Liu, C. Tao, A. Wang, W. Wei, H. Yu, Y. Wei, *Angew. Chem. Int. Ed.* 2021, **60**, 6382-6385.

[13] J. D. Sitter, A. K. Vannucci, *J. Am. Chem. Soc.* 2021, **143**, 2938-2943.

[14] Y. Zou, M. Zhang, F. Cao, J. Li, S. Zhang, Y. Qu, *J. Mater. Chem. A* 2021, **9**, 19692-19697.

[15] A. Saha, S. Payra, B. Selvaratnam, S. Bhattacharya, S. Pal, R. T. Koodali, S. Banerjee, *ACS Sustainable Chem. Eng.* 2018, **6**, 11345-11352.

[16] L. Kaur, M. Kumar, V. Bhalla, *Green Chem.* 2023, **25**, 5240-5246.

[17] S. Agarwal, B. Dowara, S. Kumar, V. Kumar, K. Deori, *ACS Omega*, 2022, **7**, 48615-48622.

[18] B. Dutta, S. Biswas, V. Sharma, N. O. Savage, S. P. Alpay, S. L. Suib, *Angew. Chem. Int. Ed.* 2016, **55**, 2171-2175.

[19] S. Cai, H. Rong, X. Yu, X. Liu, D. Wang, W. He, Y. Li, *ACS Catal.* 2013, **3**, 478-486.

[20] C. Zhang, N. Jiao, *Angew. Chem. Int. Ed.* 2010, **49**, 6174-6177.

[21] A. Grirrane, A. Corma, H. García, *Science*, 2008, **322**, 1661-1664.